# Chiral Design of Tough Spring-Shaped Hydrogels for Smart Umbrellas

*Mingqi Chen*[a,b], *Guangjie Song*[c], *Bin Ren*[a,*], *Lin Cai*[a], *Mokarram Hossain*[d,*], *and Chunyu Chang*[a,b,*]

[a] Department of Orthopedics, Zhongnan Hospital of Wuhan University, Wuhan 430070, China

[b] College of Chemistry and Molecular Sciences, Wuhan University, Wuhan 430072, China

[c] CAS Key Laboratory of Engineering Plastics, Institute of Chemistry, Chinese Academy of Sciences, Beijing 100190, China

[d] Zienkiewicz Institute for Modelling, Data and AI, Faculty of Science and Engineering, Swansea University, SA1 8EN Swansea, United Kingdom

*Corresponding authors

Prof. Chunyu Chang

Email: changcy@whu.edu.cn (C. Chang)

ORCID: 0000-0002-3531-5964 (C. Chang)

Dr. Bin Ren

Email: bin.ren@whu.edu.cn

Prof. Mokarram Hossain

Email: mokarram.hossain@swansea.ac.uk

**ABSTRACT:** Developing hydrogel-based artificial muscles to mimic the motion of natural muscles have long attracted scientists from the perspective of materials science for potential applications in soft robotics. However, rational design of hydrogel artificial muscles with large stroke, rapid actuation speed, and high work capacity remains a major challenge. Herein, we reported two kinds of chiral spring-shaped hydrogels that were prepared *via* consecutive shaping process (e.g., stretching, twisting, folding, coiling, and fixing). By switching the chirality of coil, homochiral muscle and heterochiral muscle were obtained, respectively. Homochiral muscle could rapidly expand to 560% with an average speed of 6.7% $s^{-1}$ in response to NIR irradiation, whose maximum work capacity reached 45 J $kg^{-1}$. On contrary, heterochiral muscle contracted 69% within 1 min under NIR irradiation with a maximum work capacity of 33 J $kg^{-1}$. Interestingly, the parasol containing homochiral muscles opened autonomously during dehydration process, while the umbrellas containing heterochiral muscle could opened rapidly when water was applied. This work provided an innovative strategy for developing tough hydrogel muscles with opposite chiralities.

**KEYWORDS:** Tough hydrogel, chirality, artificial muscle, high stroke, smart umbrella

## 1. Introduction

Thanks to their similarity with natural muscles (e.g., softness, high water content, and biocompatibility) and responsiveness to external stimuli (e.g., temperature, light, solvent, etc.), hydrogels are attractive candidates for artificial muscles, which have been applied in various fields such as soft robotics, prosthetic limbs, and smart devices [1-7]. Compared with artificial muscles composed of polymer fibers [8-10], elastomers [11-14], and carbon materials [15, 16], hydrogels possess adequate scale of deformations and good biocompatibility, thanks to the abundant presence of water enabling exchanges between hydrogel networks and external environments under stimuli [17]. However, hydrogels with homogeneous structure usually exhibit isotropic swelling and shrinking, which could not meet the controllable deformation of artificial muscles, such as linear expansion/contraction, bending, and torsion [18]. Inspired by the well-defined anisotropic structure, complex morphing, and sophisticated motions of natural organisms, hydrogels with highly ordered structure have been developed, which provided opportunity for the construction of artificial muscles with multimodal locomotion capabilities [19, 20].

Rational design of structure and shape of hydrogels would be conducive to achieve large stroke, fast actuation, and high work capacity of artificial muscles. For example, spring-shaped hydrogel could realize large deformation that could be controlled by the index, pitch, and pitch angles of spring [21]. Despite the fact that these hydrogels showed magnified deformation and improved sensitivity driven by external stimuli,

61 their soft and wet characteristics restricted them to work like skeletal muscles. Recently,
62 material scientists developed a series of fiber-shaped actuators with twisted and coiled
63 geometries, which exhibited high energy densities [15, 22-24]. After inserting twist into
64 hydrogel fibers, their load-maximized work capacity reached 11.8 J $kg^{-1}$ at the applied
65 stress of 110 kPa [25]. Although the twisted design of hydrogel muscles could store
66 mechanical energy into fibers to achieve motion, their work capacity could not reach
67 the level of natural muscles (40 J $kg^{-1}$) [25, 26]. Double-helix actuators have been
68 constructed by using two swellable twisted hydrogel fibers, whose contraction stroke
69 reached 9% in addition to a long response time of 500 s during the hydration process
70 [27]. Two-ply twisted poly(acrylic acid) fibers converted to DNA-like supercoils by
71 swelling, exhibiting a large contraction stroke (90%) but demonstrated a low actuation
72 speed (0.9% $s^{-1}$) [28]. The twisted sericin-protein hydrogel fibers exhibited high-stroke
73 (80%) and high-work capacity (73 J $kg^{-1}$) under humidity stimuli, accompanied by an
74 average speed of 3% $s^{-1}$ [29]. Spring-shaped hydrogel fibers with inserted twists could
75 rapidly contract to 90% with a contraction speed of 4.5% $s^{-1}$ during hydration process,
76 but the contraction work was only 26.2 J $kg^{-1}$ [30]. Therefore, the combination of large
77 stroke, fast actuation and high work capacity into hydrogel artificial muscles is still an
78 open issue hindering their practical applications.

79 In this work, we demonstrated a chiral design of spring-shaped artificial muscles
80 composed of double-stranded hydrogel fibers. Firstly, highly stretchable hydrogel
81 fibers were prepared by incorporating tunicate cellulose nanocrystals (TCNCs) and

PF127-DA micelles into polymeric networks. Subsequently, the hydrogel fibers were shaped through a consecutive stretching, twisting, folding, and coiling process. Finally, the spring-shaped artificial muscle was fixed by the formation of $Fe^{3+}$/−$COO^-$ ionic coordination. When the chirality of hydrogel fiber twist matched the coil's chirality, the hydrogel muscle was named as a homochiral muscle. By wrapping the twisted fiber around a mandrel to reverse the relative chirality, a heterochiral muscle was obtained. The homochiral muscle that linearly expanded in response to NIR irradiation was used to design a parasol, which could spontaneously open in a sunny day. Meanwhile, the heterochiral muscle that linearly expanded under water spraying was employed to design a rain umbrella, which could open in a rainy day.

## 2. Experimental section

### *2.1 Materials*

Tunicate cellulose nanocrystals (TCNCs) were isolated from *Halocynthia roretzi Drasche*. Acrylic acid (AA), acrylamide (AM), ammonium persulfate (APS), ferric chloride hexahydrate ($FeCl_3 \cdot 6H_2O$), triethylamine, sulfuric acid ($H_2SO_4$), and sodium hydroxide (NaOH) were purchased from Sinocharm Chemical Reagent Co. Ltd., China. Acrylic chloride was supplied by Shanghai Aladdin Co. Ltd., China. Pluronic F127 (PF127), poly (ethylene glycol)-*b*-poly (propylene glycol)-*b*-poly (ethylene glycol) was obtained from Sigma-Aldrich Co. Ltd., China. Other reagents were used as received unless otherwise noted.

### *2.2 Synthesis of PF127-DA*

PF127 (2.54 g) and triethylamine (85 μL) were dissolved in anhydrous dichloromethane (20 mL) in an ice bath, degassing for 20 mins. Then, acryloyl chloride (50 μL) was slowly injected into above solution under a nitrogen environment. The reaction was performed at room temperature for 24 h. Following the reaction, the solvent was removed by rotational evaporation at 25 °C. The crude product was dissolved in deionized water and dialyzed exhaustively against deionized water for 3 days. PF127-DA was obtained by lyophilization, whose chemical structure was verified by FTIR and $^{1}$H NMR spectra (**Figure S1**).

### *2.3 Fabrication of chiral spring-shaped hydrogels*

The experimental details for the preparation of tunicate cellulose nanocrystals (TCNCs) could be found in **Supporting Information**. The original hydrogel was prepared by polymerization of AM and AA monomers in the presence of TCNCs and PF127-DA micelles. In the mixture, the total concentration of AA and AM was 20 wt% (the molar ratio of AM/AA was 3/7~7/3), the concentration of PF127-DA was from 1.5 wt% to 4.5 wt%, the concentration of TCNC was from 0.5 wt% to 1.5 wt%, and the concentration APS was 0.5 wt‰. The above mixture was injected into a polytetrafluoroethylene tube (3 mm × 120 mm) and polymerized at 55 °C for 6 h to obtain original hydrogel. Then, the original hydrogel was pre-stretched (2000%), twisted (500, 1000, 1500, and 2000 turns $m^{-1}$), and folded in half. Finally, the deformed hydrogel was coiled on a polytetrafluoroethylene tube and immersed in $FeCl_3$ aqueous

solution for 0 h, 12 h, 24 h, and 36 h, respectively, to obtain spring-shaped hydrogel.

### *2.4 Characterization*

The morphology of TCNCs was analyzed by TEM using a JEM-2100 microscope (JEOL, Japan). The surface microstructure of the hydrogel was observed by field emission scanning electron microscope (SEM) with a Zeiss SIGMA microscope (Zeiss, Germany) operated at 5 kV. Polarizing microscopy (POM) was performed using an Axio A1 polarizing microscope (Zeiss, German) to characterize the anisotropic structure of the hydrogel. The mechanical performances of hydrogel muscles were tested by a universal material testing machine with a 1000 N load cell (Instron 5967, USA) at room temperature. Raman spectroscopy and Raman mapping of hydrogels were performed using a Raman imaging microscope (Thermo Fisher Scientific, Fitchburg, WI, U.S.A.), where the multivariate curve resolution (MCR) method was applied to Raman analysis. The chemical structure of PF127-DA was characterized by $^{1}$H NMR spectroscopy using a Bruker AVANCE III HD 400 MHz spectrometer (Switzerland). The two-dimensional (2D) X-ray diffraction measurement was performed on dry hydrogels using a Xenocs Xeuss 2.0 instrument (Xenocs, France) with a Cu Kα radiation source (λ= 1.54 Å) and a 2D detector (Pilatus 300 K, pixel size 172 μm). The data acquisition time was 600 s for WAXS patterns, and 2D scattering images were obtained by analyzing with Fit2D software from European Synchronization Radiation Facility. Herman's orientation parameters ($f_c$) were calculated from the azimuthal-intensity distribution curves of the X-ray scattering

patterns according to follow **Equations**:

$$f_c = \frac{3<\cos^2\varphi>-1}{2} \quad (1)$$

$$< \cos^2\varphi >= \frac{\int_0^{\frac{\pi}{2}} \mathrm{I}(\varphi)\cos^2\varphi\sin\varphi \mathrm{d}\varphi}{\int_0^{\frac{\pi}{2}} \mathrm{I}(\varphi)\sin\varphi d\varphi} \quad (2)$$

where $\varphi$ is azimuthal angle, and $I(\varphi)$ is the 1-D intensity distribution along with $\varphi$. $<\cos^2\varphi>$ is calculated by integrating the intensity of specific $2\theta$ diffraction peak along $\varphi$, using equation (2).

The water content of swollen hydrogels was calculated according to **Equation (3)**:

$$W_{\text{water}} = \frac{M_0 - M_{\text{d}}}{M_0} \quad (3)$$

where $M_0$ and $M_{\text{d}}$ are the weights of swollen and dried hydrogels, respectively.

The actuation strain ($\varepsilon_{act}$) of the hydrogel muscle was calculated according to **Equation (4)**:

$$\varepsilon_{\text{act}} = \frac{l_{\text{act}} - l_0}{l_0} \quad (4)$$

where $l_{\text{act}}$ is the length of the hydrogel muscle after actuation and $l_0$ is the initial length of the hydrogel muscle.

Work capacity ($Q_{\text{act}}$) of the hydrogel muscle was calculated by **Equation (5)**:

$$Q_{\text{act}} = \frac{l_{\text{act}} * M_{\text{L}}}{M_0} \quad (5)$$

where $M_{\text{L}}$ is the loaded weight upon the hydrogel muscle. The equivalent diameter ($d_{\text{e}}$) of the two-ply hydrogel was calculated according to **Equation (6)**:

$$d_{\text{e}} = 2^{0.5} d \quad (6)$$

where $d$ is the diameter of the individual hydrogel fiber.

The spring index ($c$) of chiral spring-shaped hydrogel was calculated according to

**Equation (7)**:

$$c = \frac{d_c}{d_e} \quad (7)$$

where $d_c$ is the diameter of the coil of chiral spring-shaped hydrogel.

## 3. Results and discussion

### *3.1 Fabrication, morphology and structure of chiral spring-shaped hydrogels*

The original hydrogel was prepared by polymerization of acrylic acid (AA), acrylamide (AM), and PF127-DA in the presence of tunicate cellulose nanocrystals (TCNCs). PF127-DA was synthesized by modifying PF127 with acryloyl chloride in dichloromethane, whose structure was confirmed by $^{1}$H NMR and FTIR (**Figure S1**). Due to its amphiphilicity, the PF127-DA could assemble into micelles with an average diameter of 23.2 nm in an aqueous solution (**Figure S2**). After polymerization, the micelles acted as multifunctional crosslinkers in the hydrogel networks (**Figure S3**). Under large deformation, the original hydrogel could dissipate mechanical energy through the disassembly of micelles, resulting in high stretchability. Needle-like TCNCs (27.6 nm × 1.5 μm) were used as reinforcing components in hydrogel network to improve the mechanical strength of the original hydrogel (**Figure S4**). Thanks to its unique network structure, the original hydrogel could undergo various deformations, such as stretching, twisting, folding and coiling.

As illustrated in **Figure 1a**, chiral spring-shaped hydrogels were fabricated by consecutive stretching, twisting, folding, and coiling of original hydrogel, and then the deformed hydrogel was fixed in $FeCl_3$ aqueous solution. By switching the direction of

coiling, homochiral muscle and heterochiral muscle were obtained, respectively. The original hydrogel exhibited porous morphology and a nearly uniform diffraction pattern (**Figure 1b**), indicating that the TCNCs were randomly distributed in the hydrogel networks. After pre-stretching (2000%), the diameter of the hydrogel decreased sharply, the surface morphology of the hydrogel converted from isotropic to anisotropic, and the equatorial arcs of the hydrogel could be observed in WAXD pattern (**Figure 1c**). These results revealed that both hydrogel networks and TCNCs aligned along the direction of the external force. When the isobaric twist was inserted into the pre-stretched hydrogel with a rotation speed of 100 revolutions per minute (rpm), the diameter of hydrogel fiber further decreased, hydrogel networks oriented along the twisting direction, and the diffraction arcs assigned to ($1\bar{1}0$), (110) and (200) planes of TCNCs were clearer in the WAXD pattern (**Figure 1d**). A two-ply hydrogel was obtained by folding the twisted hydrogel in the middle through a self-balance process, whose pitch strongly depended on the twist density of the twisted hydrogel (**Figure S5**). The surface morphology of the hydrogel and the orientation of TCNCs changed slightly during the folding process (**Figure 1e**). Finally, the two-ply hydrogel was coiled upon a polytetrafluoroethylene tube and immersed into in a $FeCl_3$ aqueous solution, where the spring-shaped hydrogel was fixed by the formation of $-COO^-$/ $Fe^{3+}$ ionic coordination. The chemical composition of the spring-shaped hydrogel was evaluated by a Raman technology (**Figure S6**). The reconstructed Raman image that derived from multivariate curve resolution could be divided into green (OH- and NH-rich regions)

and blue (OH- and NH-poor regions) domains, which represented the characteristic regions of TCNCs and polymeric matrix, respectively, indicating the uniform distribution of TCNCs in hydrogel networks.

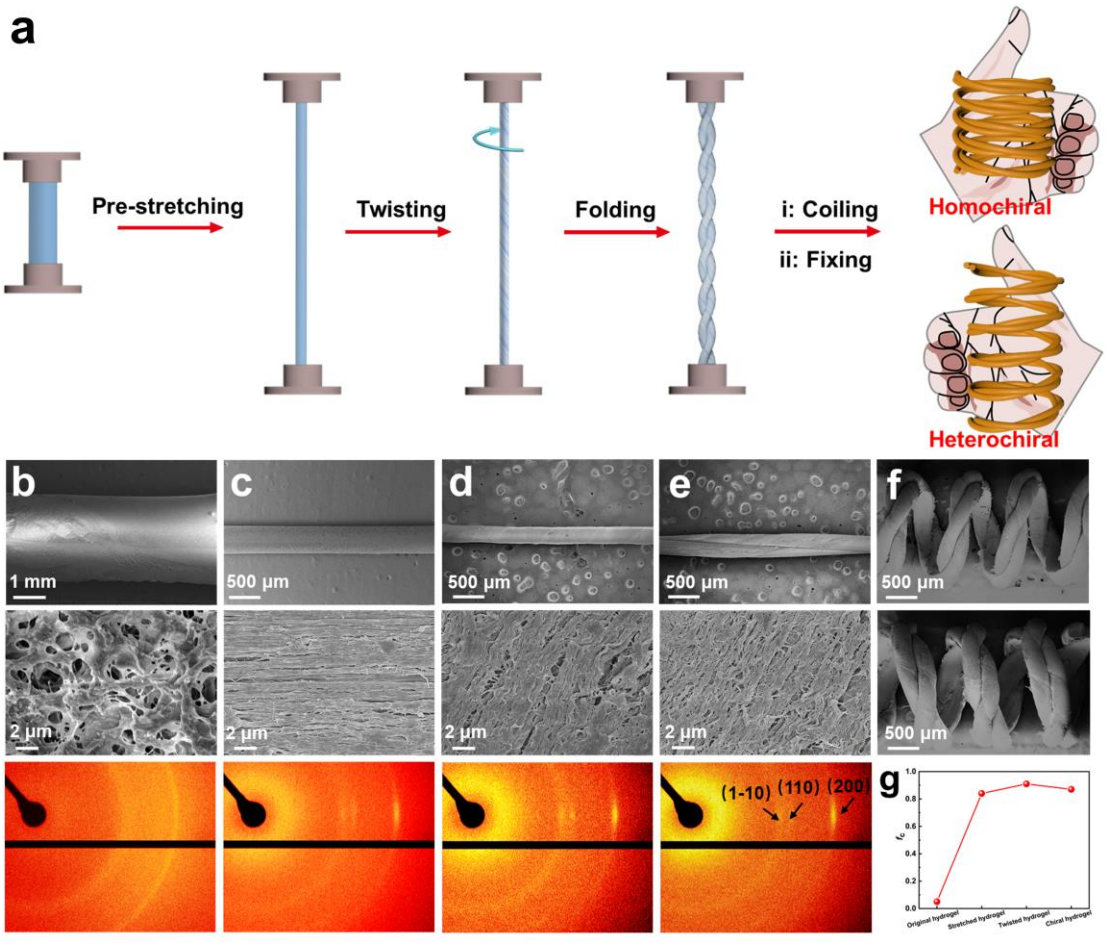


**Figure 1. Chiral design, morphology and structure of spring-shaped hydrogels.** (a) Fabrication of chiral spring-shaped hydrogels via consecutive stretching, twisting, folding, coiling and fixing process. (b-e) SEM images and WAXD patterns of hydrogels before (b) and after pre-stretching (c), twisting (d) and folding (e). (f) SEM images of homochiral hydrogel (top) and heterochiral hydrogel (bottom). (g) Influence of shaping process on orientation parameter ($f_c$) in WAXD.

When the coiling of hydrogel was in the same direction as hydrogel's twist, the spring-shaped hydrogel was defined as the homochiral muscle (**Figure 1f**, top). As the homochiral muscle was removed from the polytetrafluoroethylene tube, the untwisting of hydrogel pulled coils together (**Figure S7a**), which could be confirmed by the orientation parameter ($f_c$) value of TCNCs decreased from 0.91 to 0.87 (**Figure 1g**). Similarly, the homochiral muscle rapidly contracted along the coil axis through hydration (water spraying), whereas a linear expansion of the homochiral muscle occurred after the dehydration (NIR irradiation). On the contrary, by wrapping the twisted hydrogel around a mandrel to reverse the relative chirality, a heterochiral muscle was obtained (**Figure 1f**, bottom). The heterochiral muscle contracted under NIR irradiation due to its dehydration, which reversibly returned to the original state after water spraying (**Figure S7b**). These results revealed that chiral hydrogel muscles with opposite actuation performances were designed by changing the coiling direction of the highly twisted hydrogel fibers and then stabilizing the coils by the formation of $Fe^{3+}$/-$COO^-$ ionic coordination in the hydrogel networks.

### *3.2 Mechanical performance of various hydrogels*

Since PF127-DA micelles worked as multifunctional cross-linkers, the stretchability of the original hydrogel was dominated by the content of PF127-DA (**Figure S8**). The fracture strains of original hydrogels decreased from 2430% to 1310%, when the PF127-DA content raised from 1.5 wt% to 4.5 wt% (**Figure 2a**). This result indicated that more PF127-DA micelles increased the crosslinking density of polymeric

networks but decreased the elasticity of the original hydrogel. To ensure the high stretchability of the original hydrogel, PF127-DA content of 1.5 wt% was selected for the preparation of the original hydrogel. On the other hand, TCNCs were used as reinforcements, whose content affected the mechanical strength of hydrogel. As TCNC content increased from 0.5 wt% to 1wt%, the tensile strength of the hydrogel increased from 0.07 MPa to 0.10 MPa (**Figure 2b**). When the TCNC content exceeded 1wt%, the mechanical strength of the hydrogel decreased significantly due to the aggregation of TCNCs in hydrogel networks. Additionally, we further investigated the effects of AM/AA molar ratio on the mechanical properties of original hydrogel (**Figure 2c**). When AM/AA molar ratio was 7/3, the hydrogel had the highest toughness of 1.46 MJ $m^{-3}$, because PAM segments enabled the hydrogels with good elasticity. Therefore, the TCNC content of 1 wt% and AM/AA molar ratio of 7/3 were used to prepare the original hydrogel.

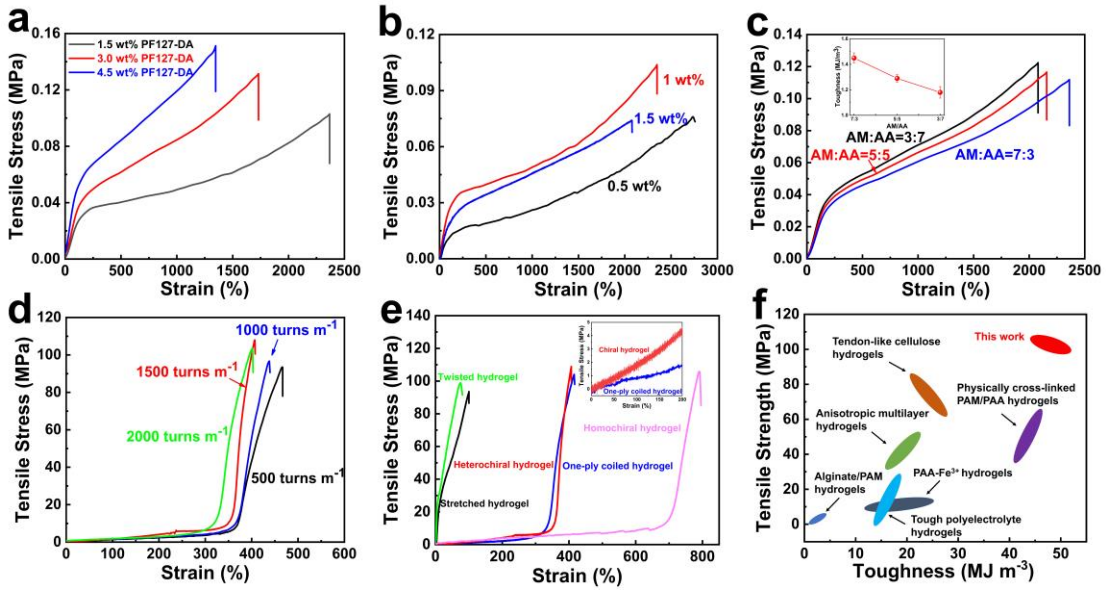

**Figure 2**. **Mechanical performance of various hydrogels.** Tensile stress-strain curves of original hydrogels with various PF127-DA content (a), TCNC content (b) and AM/AA molar ratio (c). (d) Tensile stress-strain curves of heterochiral hydrogel with various twist densities. (e) Tensile stress-strain curves of various shaped hydrogels. (f) Comparison of the tensile strength and toughness of the hydrogel muscle with reported hydrogels [31-36].

The process of twisting further improved the orientation of polymer chains and TCNCs in hydrogel networks, so the mechanical property of hydrogel strongly depended on the inserted twist density. As shown in **Figure 2d**, the chiral hydrogel with an inserted twist density of 1500 turns $m^{-1}$ showed the highest tensile strength (109 MPa), which could be attributed to the improvement of the compactness and friction of the polymer chains in hydrogel networks with an increase of the inserted twist [26]. However, a high twist density (> 1500 turns $m^{-1}$) inserted into hydrogel caused that polymer chains became increasingly oblique to the hydrogel axis, decreasing their contribution to mechanical strength along axial direction [26, 30, 37]. Additionally, the tensile stress-strain curves of various shaped hydrogels are shown in **Figure 2e** in which the tensile strength of pre-stretched hydrogel was 94.5 MPa that were further increased to 99.5 MPa after inserting twist. Compared with an one-ply coiled hydrogel (104 MPa), the tensile strength of the chiral hydrogel further increased to 109 MPa, due to the existence of internal stress and friction force in the two-ply self-balanced structure of

heterochiral hydrogel [26]. Moreover, the elastic modulus of the chiral hydrogel (1.9 MPa) was higher than that of a one-ply coiled hydrogel (1.1 MPa), which would be beneficial for the work capacity of hydrogel muscle during any actuation processes. Moreover, the mechanical property of the chiral hydrogel was compared with other reported hydrogels (**Figure 2f**). The reported hydrogels with anisotropic structures endowed them with excellent tensile strength, but their fracture strains were very low in contrast to those of the chiral hydrogel, limiting their toughness. The tensile strength and toughness of chiral hydrogel muscles were 95~109 MPa and 46.7~53.5 MJ $m^{-3}$, respectively, which were superior to those of most reported hydrogels. The stretching and twisting process not only oriented the TCNCs in hydrogel networks, but also made polymer chains compact, enhancing the mechanical performance of the chiral hydrogels.

### *3.3 Actuation performance of chiral hydrogel muscles*

The actuation mechanism of hydrogel muscles is the swelling/shrinking of polymeric networks during a hydration/dehydration process, resulting in large strokes of muscles. Taking the advantage of the network structure of the chiral hydrogels, near infrared (NIR) irradiation and water spraying were employed to achieve the dehydration and hydration of muscles, respectively. The homochiral hydrogel muscle linearly expanded under NIR irradiation and recovered after water spraying, whereas the heterochiral hydrogel muscle contracted under NIR irradiation and reversibly expanded after water spraying (**Figure S7**) due to their opposite chiralities. We investigated the

influence of different immersing time on the temperature change of hydrogel under NIR irradiation. The surface temperature of hydrogel without $Fe^{3+}$ changed slightly within 150 s. After an immersion for 12 h, the surface temperature of chiral muscles increased with the extension of NIR irradiation time, which raised from 25 to 50 ℃ within 150 s (**Figure 3a**). When the immersing time was 24 h and 36 h, the surface temperature of chiral muscles raised from 25 to 70 ℃ within 150 s under the NIR irradiation, indicating that the formation of $Fe^{3+}$/-$COO^-$ ionic coordination in network promoted photothermal conversion of hydrogel muscles, resulting in the decrease of relative humidity around the hydrogel and release of water from hydrogel muscles [38].

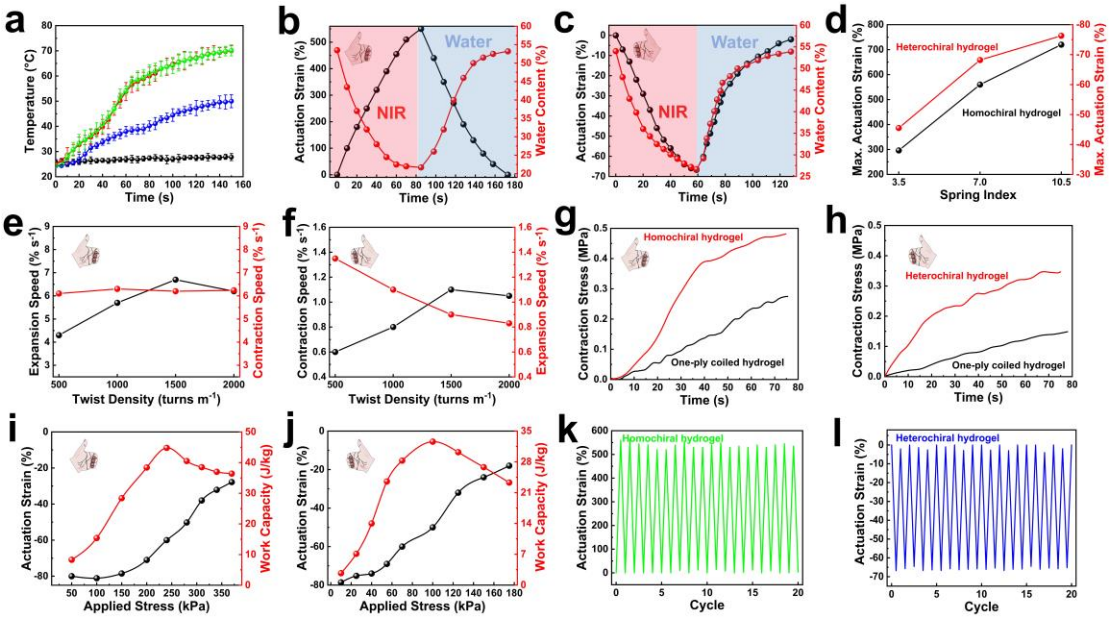


**Figure 3. Actuation performance of chiral hydrogel muscles.** (a) Temperature-time curves of hydrogels with different immersing time under NIR irradiation. Actuation strain and water content of homochiral (b) and heterochiral hydrogel (c). (d) Effects of spring index on the stroke of chiral hydrogels. Expansion and contraction speed of

homochiral (e) and heterochiral hydrogel (f) with different twist densities. Contraction stress of homochiral (g) and heterochiral hydrogel (h) is as a function of time. The dependence of the actuation strain and work capacity upon applied stress for homochiral (i) and heterochiral hydrogel (j). Cycling performance of homochiral (k) and heterochiral hydrogel (l).

The homochiral muscle could linearly expand 560% within 80 s under NIR irradiation, where its water content decreased from 54% to 21% (**Figure 3b**). After water spraying, the homochiral hydrogel muscle recovered to its original state (appearance and water content) within 95 s, revealing its reversible actuation performance. Conversely, the heterochiral muscle linearly contracted -69% within 60 s in the response to NIR irradiation because its water content decreased from 55% to 23%, which returned to its original state after water spraying for 63 s, as shown in **Figure 3c**. These results revealed that the reversible actuation of the chiral hydrogel muscles with large strokes could be achieved in the response to the NIR irradiation/water spraying. Hydrogel muscles with different chirality exhibited opposite actuation performance, where NIR irradiation induced dehydration increased the twist density of hydrogel fibers and generated a twisting torque, leading to the expansion of the homochiral muscle and the contraction of the heterochiral muscle, respectively [25]. Meanwhile, chiral hydrogel muscles could recover to their original states after hydration of polymeric networks *via* water spraying. The stroke of spring-shaped hydrogels could

334 be controlled by their spring index. As the spring index increased from 3.5 to 10.5, the
335 maximum expansion strain of the homochiral muscle increased from 295% to 720%
336 (**Figure S9a**), while the contraction strain of the heterochiral muscle increased from -
337 46% to -77% under NIR irradiation (**Figure S9b, Figure 3d**). The homochiral hydrogel
338 muscle with a spring index of 7.0 exhibited a maximum expansion speed of 6.7% $s^{-1}$
339 (**Figure S9c**), and the heterochiral hydrogel muscle with the same spring index showed
340 a maximum contraction speed of -1.1% $s^{-1}$ under NIR irradiation (**Figure S9d**).
341 The inserted twist density was another important factor affecting the actuation
342 performances of hydrogel muscles. As the inserted twist density increased from 500 to
343 2000 turn $m^{-1}$, the hydrogel fiber bias angle raised from 21.9° to 66.7° (**Figure S10**).
344 The expansion strain of the homochiral muscle monotonously increased from 350% to
345 560% (**Figure S11a**), whereas the contraction strain of the heterochiral muscle
346 increased from -57% to -69% in the response to NIR irradiation (**Figure S11b**). Besides,
347 when the inserted twist density of hydrogel fibers increased from 500 to 1500 turn $m^{-1}$,
348 the expansion speed of the homochiral hydrogel muscle increased from 4.3% $s^{-1}$ to 6.7 %
349 $s^{-1}$ under NIR irradiation, but its contraction speed basically maintained at -6.2% $s^{-1}$
350 after water spraying (**Figure 3e**), because the actuation strains increased with a rise of
351 the inserted twist density, which improved the average expansion speed of chiral
352 hydrogels during dehydration process, but the hydration time of hydrogel networks with
353 a higher twist density was longer during water spraying [39, 40]. The contraction speed
354 of heterochiral hydrogel muscle increased from -0.6% $s^{-1}$ to -1.1% $s^{-1}$ under NIR

irradiation but its expansion speed decreased from 1.3% to 0.8% $s^{-1}$ after water spraying (**Figure 3f**), as the inserted twist density of hydrogel fiber increased from 500 to 1500 turn $m^{-1}$. It is noteworthy that the expansion speed of the homochiral muscle and the contraction speed of the heterochiral muscle decreased slightly with further increasing of inserted twist density to 2000 turn $m^{-1}$, because excessive inserted twists destroyed the oriented polymer chains [30]. We have compared the actuation performance of novel hydrogels with those reported in the literatures (**Figure S12**). Solvent-responsive hydrogel actuators had large actuation strain under external stimuli but required long actuation time [25, 41]. Carbon nanotube (CNT)-based artificial muscles showed high actuation speed, however, their actuation strains were limited during actuation because of small deformation [42, 43]. Our spring-shaped hydrogels exhibited larger stroke due to unique structure and good water exchange capacity. Moreover, the formation of $Fe^{3+}$/-$COO^-$ ionic coordination promoted photothermal conversion of hydrogels, resulting in the fast release of water from hydrogel networks and high actuation speed of hydrogels.

In addition to actuation strain and speed, work capacity is a key factor of hydrogel muscle, which was dominated by the maximum contraction stress. The contraction stress of homochiral hydrogel reached 0.47 MPa by water spraying for 100 s, which was higher than that of a one-ply hydrogel (0.24 MPa), as shown in **Figure 3g**. Similarly, the contraction stress of heterochiral hydrogel increased gradually from 0.0 to 0.35 MPa under the NIR irradiation within 75 s (**Figure 3h**). These results revealed that chiral

muscles had higher contraction stress in comparison with a one-ply hydrogel. Benefiting from their excellent contraction stress, the chiral hydrogels could be used to lift objects under the NIR irradiation and water spraying (**Movie S1**, **S2**). The actuation strain and work capacity as a function of the applied stress for homochiral muscle are shown in **Figure 3i**. When the applied stress increased from 50 kPa to 350 kPa, the actuation strain of homochiral muscle changed from -81% to -30% under water spraying. The maximum work capacity of the homochiral muscle reached 45 J $kg^{-1}$ with an applied load of 250 kPa. For the heterochiral muscle, its actuation strain decreased from -79% to -20% with the increase of the applied stress from 10 kPa to 180 kPa in response to the NIR irradiation (**Figure 3j**). The maximum work capacity of heterochiral muscle was 33 J $kg^{-1}$ at the applied stress of 100 kPa, which was much higher than the reported hydrogel muscle [25], because the two-ply design of hydrogel had higher contraction stress in comparison with the one-ply hydrogel. Chiral hydrogel muscles with an inserted twist density of 1500 turns $m^{-1}$ exhibited the highest work capacity, which was consisted with the results of tensile strength and actuation speed. Moreover, the homochiral hydrogel muscle showed a large stroke of ~540% even after 20 dehydration/hydration cycles (**Figure 3k**), while the contractile stroke of the heterochiral hydrogel muscle could maintain at ~65% (**Figure 3l**). The hydrogel muscles exhibited stable appearance and morphology after 20 repeated actuations (**Figure S13**). These results revealed that the actuations of chiral hydrogel muscles were reversible and repeatable, indicating good stability of hydrogel muscles, which was

conductive to their practical applications.

### *3.4 Application of chiral hydrogel muscles*

According to their excellent mechanical properties, good actuation performances, opposite chirality, homochiral and heterochiral hydrogel muscles were employed to design the parasol and rain umbrella, respectively. **Figure 4a** shows the schematic diagram of parasol model with homochiral hydrogel muscle, where the parasol was expected to automatically open in a sunny day. Under NIR irradiation, homochiral hydrogel muscle could rapidly expand through a dehydration process, thus opening the parasol (**Figure 4b**). Reversibly, the parasol returned to its closed state after spraying water or increasing ambient humidity, because the homochiral hydrogel contracted *via* hydration of polymeric networks. On the other hand, the rain umbrella integrated with the heterochiral hydrogel muscle was also designed (**Figure 4c**). In a rainy day, the heterochiral hydrogel could expand through after absorbing water, leading to the opening of the rain umbrella. Under sunshine or decline of humidity, the heterochiral hydrogel contracted due to dehydration, resulting in the closing of the rain umbrella (**Figure 4d**). These results indicated that the chiral muscles could reversibly open/close the smart umbrella as the humidity of the external environment changed, revealing their potential application in the field of smart devices.

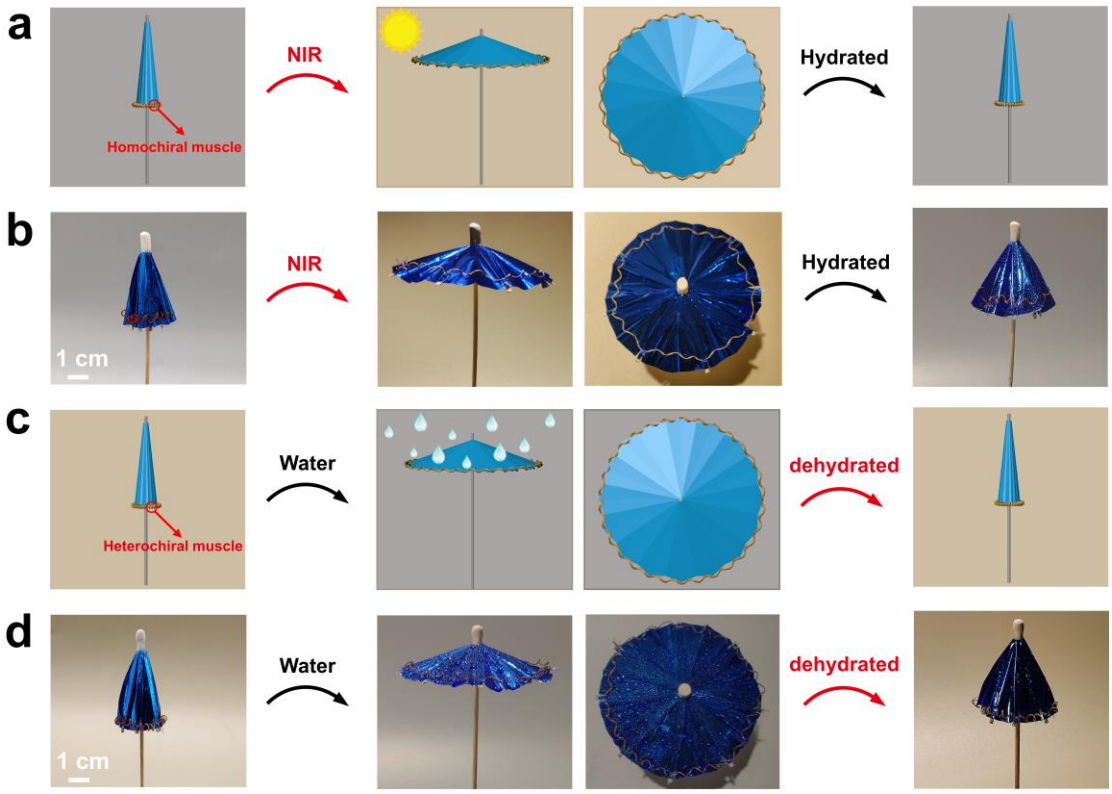


**Figure 4**. **Application of chiral hydrogel muscles.** The schematic diagram (a) and photograph (b) of the parasol containing homochiral hydrogel, and the schematic diagram (c) and photograph (d) of the rain umbrella containing heterochiral hydrogel.

## 4. Conclusion

We have successfully fabricated spring-shaped hydrogel muscles with opposite chirality through a consecutive stretching, twisting, folding, coiling, and fixing process. The presence of PF127-DA micelles that acted as multifunctional cross-linkers endowed the original hydrogels with high stretchability, while the incorporation of TCNCs significantly improved the mechanical strength of hydrogels, enabling them to undergo various large deformations. The formation of -$COO^-$/ $Fe^{3+}$ionic coordination further enhanced the crosslinking density of hydrogel networks and firmly locked the

shaped hydrogel networks. Homochiral muscle could rapidly expand to 560% with an average speed of 6.7% $s^{-1}$ under an NIR irradiation, whose maximum work capacity reached 45 J $kg^{-1}$. By contrary, heterochiral muscle contracted 69% within 1 min under NIR irradiation with a maximum work capacity of 33 J $kg^{-1}$. Thanks to their excellent mechanical properties, high stroke, high actuation speed, and high work capacity, chiral hydrogel muscles were used to design smart umbrellas, where homochiral muscle could spontaneously open the parasol under NIR irradiation and heterochiral muscle could open rain umbrella by spraying water. This work provided an innovative strategy for developing tough hydrogel muscles with opposite chiralities which could have potential applications in the field of smart umbrellas.

## Declaration of Competing Interest

The authors declare that they have no known competing financial interests or personal relationships that could have appeared to influence the work reported in this paper.

## Acknowledgments

This work was financially supported by the National Key Research and Development Program of China (2018YFE0123700), the National Natural Science Foundation of China (52073217, 51873164), and Key Research and Development Program of Hubei Province (2020BCA079).

## Appendix A. Supplementary data

Supplementary data to this article can be found online.

## References


[1] H. Na, Y.W. Kang, C.S. Park, S. Jung, H.Y. Kim, J.Y. Sun, Hydrogel-based strong and fast actuators by electroosmotic turgor pressure, Science 376(6590) (2022) 301-307.

[2] Y. Ma, M. Hua, F. Zhou, X. He, Bioinspired high-power-density strong contractile hydrogel by programmable elastic recoil, Sci. Adv. 6 (2020) eabd2520.

[3] C. Lang, E.C. Lloyd, K.E. Matuszewski, Y. Xu, V. Ganesan, R. Huang, M. Kumar, R.J. Hickey, Nanostructured block copolymer muscles, Nat. Nanotechnol. 17(7) (2022) 752-758.

[4] Z. Wang, C. Valenzuela, J. Wu, Y. Chen, L. Wang, W. Feng, Bioinspired freeze-tolerant soft materials: Design, properties, and applications, Small 18(37) (2022) 2201597.

[5] P. Xue, H.K. Bisoyi, Y. Chen, H. Zeng, J. Yang, X. Yang, P. Lv, X. Zhang, A. Priimagi, L. Wang, X. Xu, Q. Li, Near-infrared light-driven shape-morphing of programmable anisotropic hydrogels enabled by mxene nanosheets, Angew. Chem., Int. Ed. 60(7) (2021) 3390-3396.

[6] X. Zhang, P. Xue, X. Yang, C. Valenzuela, Y. Chen, P. Lv, Z. Wang, L. Wang, X. Xu, Near-infrared light-driven shape-programmable hydrogel actuators loaded with metal‐organic frameworks, ACS Appl. Mater. Interfaces 14(9) (2022) 11834-11841.

[7] P. Xue, C. Valenzuela, S. Ma, X. Zhang, J. Ma, Y. Chen, X. Xu, L. Wang, Highly conductive MXene/PEDOT:PSS-integrated poly (*N*-isopropylacrylamide hydrogels for bioinspired somatosensory soft actuators, Adv. Funct. Mater. (2023) 2214867.

[8] C.S. Haines, M.D. Lima, N. Li, G.M. Spinks, J. Foroughi, B.J. Swedlove, G.G. Wallace, R.H. Baughman, Artificial muscles from fishing line and sewing thread, Science 343 (2014) 868-872.

[9] P. Xue, Y. Chen, Y. Xu, C. Valenzuela, X. Zhang, H.K. Bisoyi, X. Yang, L. Wang, X. Xu, Q. Li, Bioinspired MXene-based soft actuators exhibiting angle-independent structural color, Nano-Micro. Lett. 15(1) (2022) 1-13.

[10] Y. Chen, C. Valenzuela, X. Zhang, X. Yang, L. Wang, W. Feng, Light-driven dandelion-inspired microfliers, Nat. Commun. 14(1) (2023) 3036.

[11] Y. Chen, H. Zhao, J. Mao, P. Chirarattananon, E.F. Helbling, N.P. Hyun, D.R. Clarke, R.J. Wood, Controlled flight of a microrobot powered by soft artificial muscles, Nature 575(7782) (2019) 324-329.

[12] J. Ma, Y. Yang, C. Valenzuela, X. Zhang, L. Wang, W. Feng, Mechanochromic, Shape-programmable and self-healable cholesteric liquid crystal elastomers enabled by dynamic covalent boronic ester bonds, Angew. Chem., Int. Ed. 61(9) (2022) e202116219.

[13] M. Yang, Y. Xu, X. Zhang, H.K. Bisoyi, P. Xue, Y. Yang, X. Yang, C. Valenzuela, Y. Chen, L. Wang, W. Feng, Q. Li, Bioinspired phototropic MXene-reinforced soft tubular actuators for omnidirectional light-tracking and adaptive photovoltaics, Adv. Funct. Mater. 32(26) (2022) 2201884.

[14] X. Yang, C. Valenzuela, X. Zhang, Y. Chen, Y. Yang, L. Wang, W. Feng, Robust integration of polymerizable perovskite quantum dots with responsive polymers enables 4D-printed self-deployable information display, Matter 6(4) (2023) 1278-1294.

[15] M. Kanik, S. Orguc, G. Varnavides, J. Kim, T. Benavides, D. Gonzalez, T. Akintilo, C.C. Tasan, A.P. Chandrakasan, Y. Fink, P. Anikeeva, Strain-programmable fiber-based artificial muscle, Science 365 (2019) 145-150.

493 [16] J. Yang, X. Zhang, X. Zhang, L. Wang, W. Feng, Q. Li, Beyond the visible: Bioinspired infrared
494 adaptive materials, Adv. Mater. 33(14) (2021) 2004754.
495 [17] N. Park, J. Kim, Hydrogel-based artificial muscles: Overview and recent progress, Adv. Intell.
496 Syst. 2(4) (2020) 1900135.
497 [18] S.M. Mirvakili, I.W. Hunter, Artificial muscles: Mechanisms, applications, and challenges,
498 Adv. Mater. 30(6) (2018) 1704407.
499 [19] Z. Zhao, R. Fang, Q. Rong, M. Liu, Bioinspired nanocomposite hydrogels with highly ordered
500 structures, Adv. Mater. 29(45) (2017) 1703045.
501 [20] K. Sano, Y. Ishida, T. Aida, Synthesis of anisotropic hydrogels and their applications, Angew.
502 Chem., Int. Ed. 57(10) (2018) 2532-2543.
503 [21] K. Yoshida, S. Nakajima, R. Kawano, H. Onoe, Spring-shaped stimuli-responsive hydrogel
504 actuator with large deformation, Sens. Actuators B Chem. 272 (2018) 361-368.
505 [22] J. Mu, M. Jung de Andrade, S. Fang, X. Wang, E. Gao, N. Li, S.H. Kim, H. Wang, C. Hou, Q.
506 Zhang, M. Zhu, D. Qian, H. Lu, D. Kongahage, S. Talebian, J. Foroughi, G. Spinks, H. Kim, T.H.
507 Ware, H.J. Sim, D.Y. Lee, Y. Jang, S.J. Kim, R.H. Baughman, Sheath-run artificial muscles, Science
508 365(6449) (2019) 150-155.
509 [23] J. Yuan, W. Neri, C. Zakri, P. Merzeau, K. Kratz, A. Lendlein, P. Poulin, Shape memory
510 nanocomposite fibers for untethered high-energy microengines, Science 365(6449) (2019) 155-158.
511 [24] S. Tawfick, Y. Tang, Stronger artificial muscles, with a twist, Science 365(6449) (2019) 125-
512 126.
513 [25] Y. Cui, D. Li, C. Gong, C. Chang, Bioinspired shape memory hydrogel artificial muscles driven

514 by solvents, ACS Nano 15 (2021) 13712-13720.

515 [26] X. Zhou, S. Fang, X. Leng, Z. Liu, R.H. Baughman, The power of fiber twist, Acc. Chem. Res.

516 54 (2021) 2624-2636.

517 [27] D.J. Shepherd, G.M. Spinks, Double helix actuators, Adv. Mater. Technol. 4(1) (2019) 1800525.

518 [28] G.M. Spinks, N.D. Martino, S. Naficy, D.J. Shepherd, J. Foroughi, Dual high-stroke and high-

519 work capacity artificial muscles inspired by DNA supercoiling, Sci. Robot. 6(53) (2021) eabf4788.

520 [29] T. Jia, Y. Wang, Y. Dou, Y. Li, M.J.d. Andrade, R.H. Baughman, D. Qian, Z. Liu, Moisture

521 sensitive smart yarns and textiles from self-balanced silk fiber muscles, Adv. Funct. Mater. 29 (2019)

522 1808241.

523 [30] C. You, W. Qin, Z. Yan, Z. Ren, J. Huang, J. Ii, W. Chang, W. He, K. Wen, S. Yin, X. Zhou, Z.

524 Liu, Highly improved water tolerance of hydrogel fibers with a carbon nanotube sheath for

525 rotational, contractile and elongational actuation, J. Mater. Chem. A 9(16) (2021) 10240-10250.

526 [31] Y.Z. Guo, T. Nakajima, M.T.I. Mredha, H.L. Guo, K. Cui, Y. Zheng, W. Cui, T. Kurokawa, J.P.

527 Gong, Facile preparation of cellulose hydrogel with achilles tendon-like super strength through

528 aligning hierarchical fibrous structure, Chem. Eng. J. 428 (2022) 132040.

529 [32] T. Zhang, T. Zuo, D. Hu, C. Chang, Dual physically cross-linked nanocomposite hydrogels

530 reinforced by tunicate cellulose nanocrystals with high toughness and good self-recoverability, ACS

531 Appl. Mater. Interfaces 9(28) (2017) 24230-24237.

532 [33] D. Hu, Y. Cui, K. Mo, J. Wang, Y. Huang, X. Miao, J. Lin, C. Chang, Ultrahigh strength

533 nanocomposite hydrogels designed by locking oriented tunicate cellulose nanocrystals in polymeric

534 networks, Compos. B. Eng. 197 (2020) 108118.

[34] M.T.I. Mredha, H.H. Le, V.T. Tran, P. Trtik, J. Cui, I. Jeon, Anisotropic tough multilayer hydrogels with programmable orientation, Mater. Horiz. 6 (2019) 1504-1511.

[35] S. Choi, Y. Choi, J. Kim, Anisotropic hybrid hydrogels with superior mechanical properties reminiscent of tendons or ligaments, Adv. Funct. Mater. 29(38) (2019) 1904342.

[36] F. Luo, T.L. Sun, T. Nakajima, T. Kurokawa, Y. Zhao, K. Sato, A.B. Ihsan, X. Li, H. Guo, J.P. Gong, Oppositely charged polyelectrolytes form tough, self-healing, and rebuildable hydrogels, Advanced Materials 27(17) (2015) 2722-2727.

[37] M. Zou, S. Li, X. Hu, X. Leng, R. Wang, X. Zhou, Z. Liu, Progresses in tensile, torsional, and multifunctional soft actuators, Adv. Mater. 31 (2021) 2007437.

[38] Y. Liu, Z. Zhang, Z. Liang, Y. Yong, C. Yang, Z. Li, Multifunctional polyurethane hydrogel based on a phenol-carbamate network and an $Fe^{3+}$-polyphenol coordination bond toward nir light triggered actuators and strain sensors, J. Mater. Chem. A 10 (2022) 16928-16940.

[39] Y. Wang, Z. Wang, Z. Lu, M. Jung de Andrade, S. Fang, Z. Zhang, J. Wu, R.H. Baughman, Humidity- and water-responsive torsional and contractile lotus fiber yarn artificial muscles, ACS Appl. Mater. Interfaces 13(5) (2021) 6642-6649.

[40] H. Cheng, Y. Hu, F. Zhao, Z. Dong, Y. Wang, N. Chen, Z. Zhang, L. Qu, Moisture-activated torsional graphene-fiber motor, Adv. Mater. 26(18) (2014) 2909-2913.

[41] H.J. Sim, Y. Jang, H. Kim, J.G. Choi, J.W. Park, D.Y. Lee, S.J. Kim, Self-helical fiber for glucose-responsive artificial muscle, ACS Appl. Mater. Interfaces 12(18) (2020) 20228-20233.

[42] Y. Wang, J. Qiao, K. Wu, W. Yang, M. Ren, L. Dong, Y. Zhou, Y. Wu, X. Wang, Z. Yong, J. Di, Q. Li, High-twist-pervaded electrochemical yarn muscles with ultralarge and fast contractile

actuations, Mater. Horiz. 7(11) (2020) 3043-3050.

[43] J.A. Lee, N. Li, C.S. Haines, K.J. Kim, X. Lepro, R. Ovalle-Robles, S.J. Kim, R.H. Baughman, Electrochemically powered, energy-conserving carbon nanotube artificial muscles, Adv. Mater. 29(31) (2017) 1700870.